https://doi.org/10.5194/egusphere-2023-1412
Preprint. Discussion started: 4 August 2023

Causal associations and predictability of the summer East Atlantic teleconnection

Julianna Carvalho-Oliveira[1,2,3], Giorgia di Capua[4,5], Leonard Borchert[1], Reik Donner[5,4], and Johanna Baehr[1]

[1]Institute of Oceanography, Center for Earth System Research and Sustainability (CEN), Universität Hamburg, Hamburg, Germany
[2]International Max Planck Research School on Earth System Modelling, Max Planck Institute for Meteorology, Hamburg, Germany
[3]Helmholtz-Zentrum Hereon, Institute of Coastal Systems - Analysis and Modeling, Geesthacht, Germany
[4]Potsdam Institute for Climate Impact Research, Member of the Leibniz Association, Potsdam, Germany
[5]Department of Water, Environment, Construction and Safety, Magdeburg-Stendal University of Applied Sciences, Magdeburg, Germany

Correspondence: Julianna Carvalho-Oliveira (julianna.carvalho.oliveira@uni-hamburg.de)

Abstract.

We apply Causal Effect Networks to evaluate the influence of spring North Atlantic extratropical surface temperatures (SST) on the summer East Atlantic Pattern (EA) seasonal predictability during the 20th century. We find in the ERA-20C reanalysis that a meridional SST gradient in spring (SST index) causally influences the summer EA, with an estimated causal effect expressed by a β-coefficient of about 0.2 (a 1 standard deviation change in spring SST index causes a 0.2 standard deviation change in the EA 3-4 months later). We only find this link to be causal, however, during the period 1958 - 2008. When performing the analysis on 45-year-long timeseries randomly sampled in this late period, we find the strength of the causal link to be affected by interannual variability, suggesting a potential modulation by an external physical mechanism. In addition to the summer EA, we find that spring SST has an estimated causal effect of about -0.2 on summer 2-metre air temperatures over northwestern Europe, possibly mediated by summer EA. We then use a pre-industrial and a historical simulation, as well as a 30-member initialised seasonal prediction ensemble with MPI-ESM-MR to test the model performance in reproducing the detected causal links in ERA-20C and to evaluate whether this performance might leave an imprint in the model predictive skill of European summer climate. We find that while MPI-ESM-MR is mostly unable to reproduce the causal link between spring SST and the summer EA among the different datasets, the 30-member initialised ensemble can moderately reproduce a causal link between spring SST and summer 2-metre air temperatures over a region west of the British Isles. We perform a predictive skill assessment conditioned on the spring SST causal links for July-August sea level pressure, 500 hPa geopotential height and 2-metre air temperatures for predictions initialised in May. Our results suggest that MPI-ESM-MR's performance in reproducing the spring SST causal links constrains the seasonal prediction skill of European summer climate.

https://doi.org/10.5194/egusphere-2023-1412
Preprint. Discussion started: 4 August 2023

1 Introduction

The summer East Atlantic Pattern (EA) is an important atmospheric teleconnections influencing weather and climate in the Euro-Atlantic region (e.g. Comas-Bru and McDermott (2014); Bastos et al. (2016)). Along with the summer North Atlantic Oscillation (NAO), these teleconnections are often used to describe the combined changes in latitude and speed of the North Atlantic jet stream (Woollings et al., 2010) – one of the major modulators of mid-latitude weather extremes (e.g. Rousi et al. (2022)). Understanding the predictability associated with these teleconnections is therefore of paramount importance. Although several recent studies have focused on predictability of the NAO (Domeisen et al., 2018; O'Reilly et al., 2019; Athanasiadis et al., 2020; Klavans et al., 2021), the EA has received less attention. Here, we apply a causal inference-based tool to evaluate the influence of North Atlantic extratropical surface temperatures (SST) on the predictability of EA at seasonal timescales.

The most common description of the EA pattern features a well-defined sea level pressure (SLP) centre of action south of Iceland and west of the British Isles, usually defined as the second leading empirical orthogonal function (EOF) of SLP in the Euro-Atlantic region (e.g. Moore et al. (2013)). Wallace and Gutzler (1981) define a positive phase of the EA as characterised by the centre of action exhibiting anticyclonic conditions, featuring the northward extension of the Azores High. A positive EA has been associated with below-average surface temperatures (Cassou et al., 2005; Comas-Bru and Hernández, 2018) and dry spells in parts of Europe (Rousi et al., 2021). Conversely, anomalous cyclonic conditions offshore of Ireland have been suggested to influence heatwaves in Europe for a negative EA phase (e.g. Duchez et al. (2016)). Using a clustering approach (e.g. Cassou et al. (2004); Carvalho-Oliveira et al. (2022)), a positive EA phase is reminiscent of an Atlantic Ridge, whereas a negative EA phase resembles the Atlantic Low. A common feature amongst the different EA definitions is that its centre of action is positioned along the NAO nodal line, thus ultimately modulating the location and strength of the NAO dipole and the North Atlantic storm track (Woollings et al., 2010). That is, summer climate predictability in the Euro-Atlantic region is closely linked to EA variability.

While there is no consensus on the physical processes driving the EA, spring North Atlantic sea surface temperatures (SSTs) have been proposed to influence EA variability and predictability. Gastineau and Frankignoul (2015) suggested that summer 500-hPa geopotential height anomalies in the Euro-Atlantic significantly co-vary with a spring North Atlantic SST tripole pattern in observations over the 20th century. Moreover, Carvalho-Oliveira et al. (2022) suggested that spring North Atlantic SSTs can influence predictive skill of summers dominated by EA in initialised simulations. Based on linear regression analyses of the period 1979–2017, Ossó et al. (2018) and Ossó et al. (2020) proposed a physical mechanism whereby anomalous extratropical North Atlantic SSTs in spring may persist into summer and influence shifts in the eddy-driven jet stream, imprinting at the surface an SLP pattern that resembles the EA. These studies suggest that this mechanism is forced by changes in baroclinicity of the lower troposphere associated with a strong meridional SST gradient in spring located between subpolar and subtropical North Atlantic. The authors hypothesised that the delayed atmospheric response in summer, and not in spring, could be explained by the seasonal evolution of both SST gradient and jet stream position, modulated by a positive coupled ocean–atmosphere feedback that operates primarily in summer.

https://doi.org/10.5194/egusphere-2023-1412
Preprint. Discussion started: 4 August 2023

Nevertheless, while the linear regression-based analysis provided in Ossó et al. (2018) suggests a contribution of spring SST on the summer SLP variability, this approach does not imply causation. Disentangling the complex causal-effect pathways underlying the mechanism proposed in Ossó et al. (2020) over a long observational record is a crucial step to evaluate EA predictability in dynamical climate models. Hence, in this paper we use Causal Effect Network (CEN, Runge et al. (2015); Kretschmer et al. (2016)) to test the hypothesis of spring SST causally driving a response in the summer SLP and temperature fields in the Euro-Atlantic sector during the 20th century. CEN overcomes spurious correlations due to autocorrelation, indirect effects, or common drivers (Runge et al., 2019), and has been successfully used to complement hypothesis testing for other teleconnections (e.g. Di Capua et al. (2020a)).

Although dynamical seasonal forecasts of European summer climate usually show very little skill (e.g. Mishra et al. (2019)), recent studies suggest that improving the representation of teleconnections can increase forecast skill (Oliveira et al., 2020; Carvalho-Oliveira et al., 2022; Schuhen et al., 2022). The physical mechanism connecting SST variability and jet stream dynamics proposed in Ossó et al. (2020) thus offers a framework to more generally assess the influence of SST on seasonal predictability of the EA – the aim of the present study.

Here, we use CEN to firstly investigate under which circumstances spring extratropical North Atlantic SSTs causally influence the summer EA and its associated impact on surface climate. Secondly, we analyse pre-industrial, historical and initialised simulations with the Max Planck Institute Earth System Model in its mixed-resolution setup MPI-ESM-MR (MPI-ESM-MR, Dobrynin et al. (2018)). We specifically test the model performance in reproducing the observed SST - EA link, in order to identify how this performance might constrain the seasonal prediction skill of European summer climate.

2 Methodology

2.1 Reanalysis and model data

We investigate the SST - EA link first using ERA-20C reanalysis (Poli et al., 2016), and then using model simulations with MPI-ESM-MR (Dobrynin et al., 2018)). We analyse sea level pressure, sea surface temperature (SST), and air temperature at 2 metre height (T2m). We use monthly means for each variable as we are testing mechanisms which are expected to act on monthly timescales. We focus our analysis on the 101-year long period spanning 1908-2008 in the model and observations.

In MPI-ESM-MR, the atmospheric component ECHAM6 (Stevens et al., 2013) has a resolution of T63L95, with a nominal horizontal resolution of 200 km (1.875°) and 95 vertical layers up to 0.01 hPa. The oceanic component MPI-OM (Jungclaus et al., 2013) is coupled to ECHAM6 and has a resolution of TP04L40, with an approximate horizontal resolution of 40 km (0.4°) and 40 vertical layers. External forcing is taken from CMIP5 (Giorgetta et al., 2013).

We investigate how MPI-ESM-MR performs in reproducing the SST - EA link among three independent sets of MPI-ESM-MR simulations. The datasets comprise a pre-industrial control run (piControl), a historical run, and a 30-member seasonal initialised hindcast ensemble (MR-30). Comparing the performance of each set against reanalysis enables us to distinguish the role of forcing (from piControl to historical), and of assimilation (historical to initialised ensemble) on the model skill.

https://doi.org/10.5194/egusphere-2023-1412
Preprint. Discussion started: 4 August 2023

The pre-industrial coupled atmosphere/ocean control run piControl has a total length of 1000 years (period 1850-2849) (Giorgetta et al., 2011), with forcing constant in time: orbital parameters and greenhouse gases concentration are fixed at 1850 values; spectral solar irradiance remains constant as the solar cycle average over 1844-1856, and monthly ozone concentrations are fixed at the 11-year average over 1850-1860 (Mauritsen et al., 2012). The historical simulations run from 1850 to 2005 under natural and anthropogenic forcing following CMIP5 protocol (Dobrynin et al., 2018).

Lastly, the hindcast ensemble MR-30 is initialised on 1st of May every year from 1902-2008, with initial conditions taken from an assimilation experiment (Oliveira et al., 2020). In the assimilation experiment, Newtonian relaxation (*nudging*) is used in full-field mode towards all atmospheric and ocean levels except in the boundary layer. The atmosphere conditions of vorticity, divergence, three-dimensional temperature and two-dimensional pressure are assimilated with ERA-20C data. In the ocean, three-dimensional daily mean salinity and temperature anomalies are nudged at a relaxation time of approximately 10 days. The ocean state is derived in an ocean-only simulation performed with MPI-OM forced with the atmospheric variables from ERA-20C. The three-dimensional atmospheric and ocean fields of the assimilation experiment form the initial conditions, from which 30 ensemble members are generated by perturbing the atmospheric state with slightly disturbed diffusion coefficients in the uppermost layer.

2.2 Data-processing and climate indices

We compute anomalies at every gridpoint by removing mean seasonal cycle and linear trend, satisfying data input requirements for the CEN algorithm (Kretschmer et al., 2016). We analyse bimonthly means in March-April (MA) and April-May (AM) for spring SST and July-August (JA) SLP and T2m. In MR-30, we use the assimilation experiment to obtain spring SST fields, and the hindcast ensemble at lead times 3-4 months to obtain summer SLP, T2m and 500 hPa geopotential height (Z500). We apply area-weighting by multiplying each value with the cosine of its latitudinal location to take into account the dependence of the gridpoint density on latitude.

We calculate the EA index to analyse the summer EA teleconnection. As a first step, we define a reference EA index as the second principal component (PC) of the leading empirical orthogonal function (EOF) of JA anomalies of sea level pressure over the Euro-Atlantic sector 70°W-40°E, 25°-80°N calculated from the ERA-20C reanalysis data (e.g. Comas-Bru and McDermott (2014)). Next, EA index values in the model simulations from MPI-ESM-MR are calculated by projecting each ensemble member onto the EA reference EOF pattern. We consider a positive phase of the EA index when characterised by a centre of positive SLP anomalies that lies south of Iceland and west of the British Isles (e.g. Wallace and Gutzler (1981); Comas-Bru and McDermott (2014), Fig.1a).

We further test the influence of spring extratropical North Atlantic SSTs on the summer EA using the SST index proposed in Ossó et al. (2018). We calculate the SST index by subtracting the average SST over the eastern box (35°W-20°W, 35°-42°N) from the average SST over the western box (52°W-40°W, 42°-52°N), represented by green boxes in Fig.1b. We analyse the SST index for both March-April and April-May means.

https://doi.org/10.5194/egusphere-2023-1412
Preprint. Discussion started: 4 August 2023

To fully analyse the impact of spring SST on the summer SLP variability, we include the SLP index proposed in Ossó et al. (2018), in addition to the EA index. The SLP index is calculated as JA SLP anomalies averaged over the region 45°N-55°N; 25°W-5°W indicated by a blue box in Fig1b.

All climate indices are standardised to have mean of zero and SD of 1 to allow for comparison. Using the aforementioned climate indices, we perform linear regressions and correlations to analyse the linear relationship between the predictor spring SST and the target variables summer EA, SLP, and T2m$_{CE}$ indices. Wherever useful, we use a two-tailed Student's t-test to calculate the statistical significance of correlations.

2.3 Causal effect networks

We use Causal Effect Network analysis (CEN, Runge et al. (2015); Kretschmer et al. (2016)) to test whether spring SST anomalies causally influences the variability of summer SLP and temperature fields in the Euro-Atlantic sector during the 20th century. CEN analysis is a causal discovery tool which implements the so-called Peter and Clark momentary conditional independence algorithm (PC-MCI, Runge et al. (2019)). This algorithm iteratively calculates partial correlations amongst a set of time-series to test if a link between a potential precursor and a target variable at a certain time lag is: *i)* considered spurious, i.e. can be explained by the combination of other time-series at different lags (i.e. conditional independence); or *ii)* considered causal, i.e. cannot be explained by the combined influence of other investigated variables (i.e. conditional dependence). We stress, however, that the term *causal* should be interpreted as causal relative to the set of investigated variables, under the assumptions considered in the PC-MCI algorithm (e.g. stationarity of time-series). We refer the reader to Runge (2018) for a thorough description of the CEN analysis and the PC-MCI algorithm.

We visualise the output of CEN analysis as a process graph, where circles represent the investigated variables, and arrows indicate the strength and the direction of the causal links. The strength is expressed by the standardised linear regression coefficient, denoted β-coefficient, and defined as the expected change of Y_t in units of its standard deviation (SD) induced by raising $X_{t-\tau}$ by 1 SD, while keeping all other potential precursors constant. Moreover, CEN analysis outputs the autocorrelation path coefficient, which represents the causal influence of a variable on itself, as opposed to the Pearson autocorrelation.

We apply causal maps (Di Capua et al., 2020b) to investigate the causal effects of a specific variable on a given atmospheric field along latitude, longitude and time dimensions. This tool builds upon the PC-MCI algorithm and CEN approach, and provides a powerful visualisation of spatial patterns. Causal maps display β-coefficients calculated with the time series of a potential precursor and each grid point of a target atmospheric field. We refer the reader to Di Capua et al. (2020b) for a detailed explanation of this method.

https://doi.org/10.5194/egusphere-2023-1412
Preprint. Discussion started: 4 August 2023

3 Results

3.1 Characteristics of the observed link: temporal and spatial variability

The spatial pattern of the summer EA in its positive phase is characterised by large-scale cyclonic conditions, except at the anticyclonic centre of action located south of Iceland and west of the British Isles (Fig.1a). A typical surface climate imprint of the summer EA in positive phase shows below-average temperatures in continental Europe (Fig.1c) and below-average precipitation in the British Isles and northwestern Europe (Fig.1d). As a first approach to evaluate the influence of extratropical SSTs in the summer EA, we use the SST index defined in Ossó et al. (2018). A pearson correlation analysis suggests that the strength of the relationship between the SST index in spring and the EA index in summer is time dependent (Fig.1f). Considering a period of observations spanning 101 years (1908-2008), this relationship is weak (r = 0.2, Fig.1e). However, this relationship changes over time: considering only the latest 51 years (1958-2008), correlation reaches significant values (r = 0.5). The temporal variability of this relationship is well illustrated for correlations calculated using a 20-year running window, which shows a reversal in the sign of correlations starting from 1945, and highlights an increase in the strength beyond 1958 (Fig.1f). This analysis suggests that the spring SST - summer EA relationship is nonstationary. Hence, we distinguish the following three periods to scope the remaining analysis: i) *early period*: 1908 - 1957; ii) *late period*: 1958-2008, and iii) *full period*: 1908-2008.

We assess the spatial features of the SST index influence on the summer atmospheric circulation in the different periods to further explore the variability of the spring SST - summer EA relationship. We analyse bimonthly averages, i.e. April-May (AM) SST and July-August (JA) SLP means, to observe the seasonal evolution of anomalies. Correlation maps show distinct patterns in early and late periods. We find significant correlations between the precursor SST index and the summer sea level pressure (SLP) over a region in the North Atlantic which reasonably coincides with the location of the EA teleconnection centre of action during the late period (Fig.2b, c.f. Fig.1a). The location of this region seems to oscillate about 45°N, remaining south of this latitude in the early period (Fig.2a), while located northwards in the late one (Fig.2b). Surrounding this high correlation region, the sign of correlations is opposite between early and late periods. We find similar results using March-April (MA) SST means, only in weaker strength.

Regression maps further suggest that spring SST anomalies persist into summer and then influence atmospheric circulation (Fig.2d-f). Positive values of the AM SST index in spring are associated with warm summer anomalies east of Newfoundland and cool anomalies west of Iberia, leading to concomitant anticyclonic conditions in the ocean located south of Greenland. In the late period, these anticyclonic conditions coincide with the position of the EA centre of action.

Moreover, we test whether the SST index influences JA T2m via the EA. We find significant correlations between the AM SST index and JA T2m, showing a similar pattern as in Fig.1b corresponding to JA EA - T2m. We find that correlations between AM SST index and JA T2m show distinct patterns between early and late periods (Fig.2g,h). A positive phase of the SST index in spring precedes a positive phase of the summer EA (e.g. Fig.2e), which in turn can be associated with below-average temperatures, primarily over central Europe. For further investigate this relationship, we calculate a T2m$_{CE}$ index, defined as the average summer air temperatures over the central European region 46°N-55°N; 11°E-34°E, represented by the red box in

https://doi.org/10.5194/egusphere-2023-1412
Preprint. Discussion started: 4 August 2023

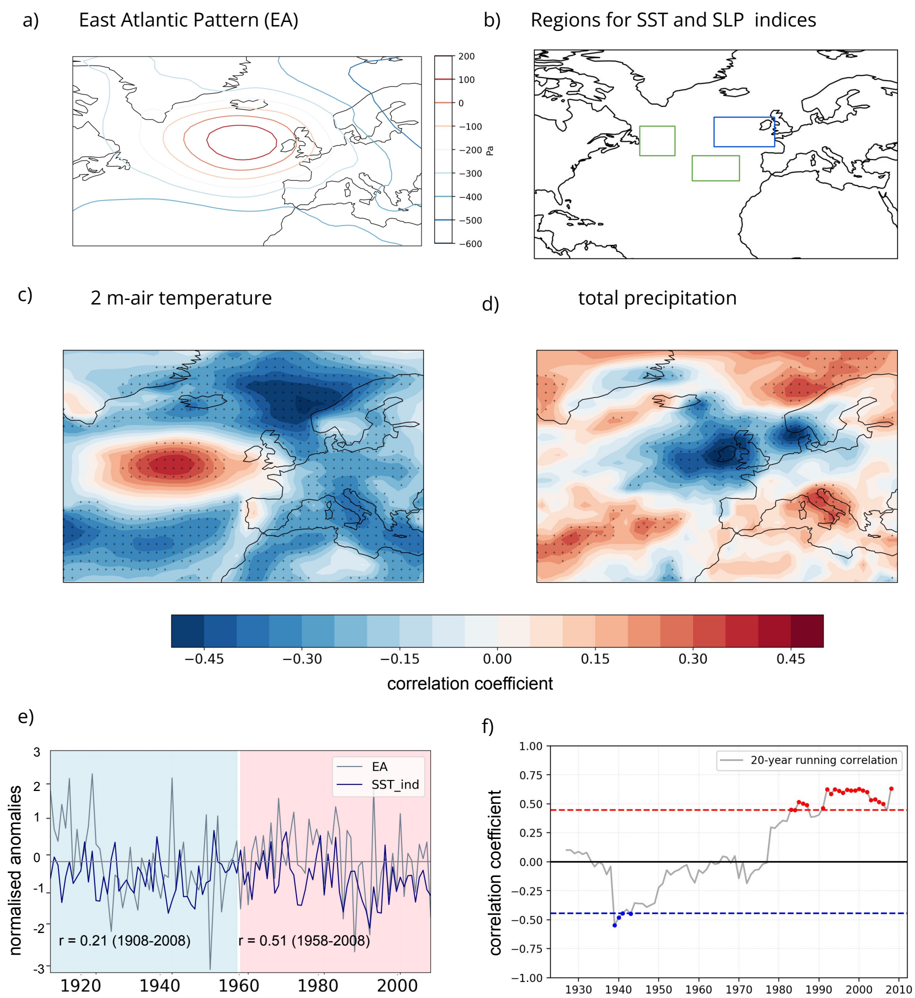

Figure 1. Variability and linear relationships of EA in ERA-20C. a) Positive phase of the EA teleconnection, defined as the second EOF of July-August SLP. b) Regions used to calculate the SST and SLP indices proposed in Ossó et al. (2018). c) Pointwise correlation of EA index with concurrent July-August anomalies of 2-metre air temperatures in the full period. d) Same as c), for July-August anomalies of total precipitation. e) Time series of SST (blue) and EA (grey) indices in ERA-20C for 1908-2008, smoothed by a 3-year running mean. f) Running-correlation between SST and EA indices for a 20-year window. Coloured markers indicate significant correlations at the 95% confidence interval, illustrated by dashed lines.

https://doi.org/10.5194/egusphere-2023-1412
Preprint. Discussion started: 4 August 2023

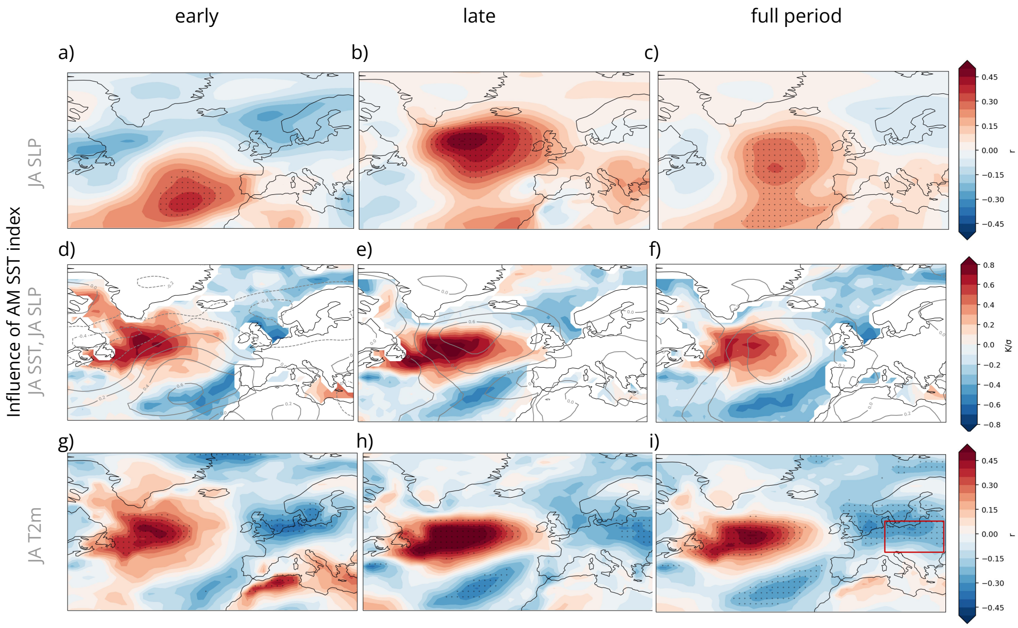

Figure 2. Distinct spatial characteristics of the spring SST influence on the summer circulation over the 20th century (for ERA-20C). Top row (a-c) shows point-wise correlation coefficients for the April-May SST index and July-August SLP means considering *early* (1908-1957), *late* (1958-2008) and *full* periods (1908-2008), respectively. Middle row (d-f) shows linear regression maps of July-August SST anomalies (shading) and SLP (contours) against the precursor SST index (normalised by the standard deviation σ). Contour interval is 0.2 hPaσ^{-1}. Bottom row (g-i) shows point-wise correlation coefficients for the April-May SST index and July-August air temperature at 2 metre height. Stippling indicates correlations significant at the 95% confidence level, calculated with a Student's t-test. Box illustrates the region used to calculate the T2m$_{CE}$ index, as described in the text.

Fig.2i. In summary, this analysis reveals that spring extratropical oceanic forcing of the summer atmospheric circulation has a marked temporal and spatial variability over the 20th century, only projecting onto the EA pattern over the late period. This variability might pose a constraint on the predictive skill of European summer climate based on spring extratropical SST during certain periods of time.

3.2 Investigating causality

To further test the robustness of the SST-EA relationship in ERA-20C, we evaluate whether spring extratropical SSTs and summer EA are conditionally dependent. Specifically, we test the hypothesis that spring SST is a causal driver for the summer EA, thus excluding autocorrelation effects or common drivers which could lead to spurious links. We perform a causality analysis using the PC-MCI algorithm (Runge et al., 2015).

First, we build one CEN for each of the three investigated periods in ERA-20C. Besides the EA and SST indices, we include two additional indices in the CEN. The first is the SLP index, defined in Ossó et al. (2018) and illustrated by the blue box in

https://doi.org/10.5194/egusphere-2023-1412
Preprint. Discussion started: 4 August 2023

Fig.1b. We thus test whether differences between early and late periods (c.f. Sec.3.1) are reflected in distinct timing or strength among the EA and SLP indices with SST. The second index concerns summer air temperatures averaged over the region represented by the red box in Fig.2i (T2m$_{CE}$), which shows significant correlations with SST. We test whether the spring SST index causally drives changes in air temperature over central Europe and under which circumstances this holds true. Our CEN analysis focuses on 3 and 4 months lag only.

Over the late period, we confirm that the spring SST index is a causal driver for both the summer EA, and the summer SLP index, at distinct time lags (Fig.3a). The strength of the causal link is expressed by the standardised regression coefficient, denoted β-coefficient in CEN. At 4-month lag, we find $\beta_{SST \to EA} \approx$ 0.22, which means that a change of 1 standard deviation (SD) in the March-April SST index leads to a change of 0.22 SD in July-August EA. We find a causal link of similar strength at 3-month lag $\beta_{SST \to SLP} \approx$ 0.21 between April-May SST and July-August EA, as well as $\beta_{SST \to T2mCE} \approx$ -0.2 between April-May SST and July-August T2m$_{CE}$. Although we speculate that the link $SST \to T2m_{CE}$ is mediated via the summer EA, we are unable to confirm this mediation with a CEN analysis focusing on 3-4 months lag. We find no significant causal links when analysing the full or early period.

Next, we test the sensitivity of the detected causal links between spring SST and summer SLP to slight differences in the analysed years. By removing 6 randomly selected years (12% of tested years in the late period) in each new CEN over 500 iterations, we test whether the causal links are particularly subjected to interannual variability (Fig.3b-e). We find high variability in the strength of the links $\beta_{SST \to EA}$ and $\beta_{SST \to SLP}$ (Fig.3b, e), ranging from zero (i.e. no causal link) to 0.5, with median values corresponding to β-coefficients calculated in Fig.3a. This sensitivity in the causal link strength due to sampling suggests that the spring SST - summer SLP relationship might be modulated by an external physical mechanism, i.e. an additional actor excluded from this CEN.

3.3 Does MPI-ESM reproduce the observed link?

We now test whether the causal links detected in ERA-20C during the late period can be reproduced by MR-30. As a first step, we compare the model ability to reproduce the temporal variability of the observed summer EA. We find that MPI-ESM is overall able to reproduce the range of variability but shows different levels of skill in reproducing the summer EA amongst the different simulation sets (Fig.4a). Historical simulations show low agreement with ERA-20C (r = 0.14), whereas MR-30 initialised simulations tend to mostly encompass the observed variability (Fig.4c).

Next, we evaluate the model skill in reproducing the spring SST - summer EA relationship. We find that the model shows limited skill, with MR-30 capturing the temporal variability of the relationship in the early, but not in the late period (Figs.4b, 5). A comparison between correlation maps computed for the evaluated periods shows that while historical simulations do not show agreement in the spatial pattern of the spring SST - summer EA relationship against observations, the MR-30 ensemble mean shows an improvement in reproducing the mechanism (Fig.5d-f). These results motivate us to assess whether the model is able to reproduce any of the observed causal links, or whether it shows different causal paths than those observed.

We build three different CEN sets to evaluate, respectively, pi-Control, historical and initialised simulations with MR-30. The variables analysed in the CEN sets are first SST, EA and SLP indices and the time lag of interest is spring - summer (3

https://doi.org/10.5194/egusphere-2023-1412
Preprint. Discussion started: 4 August 2023

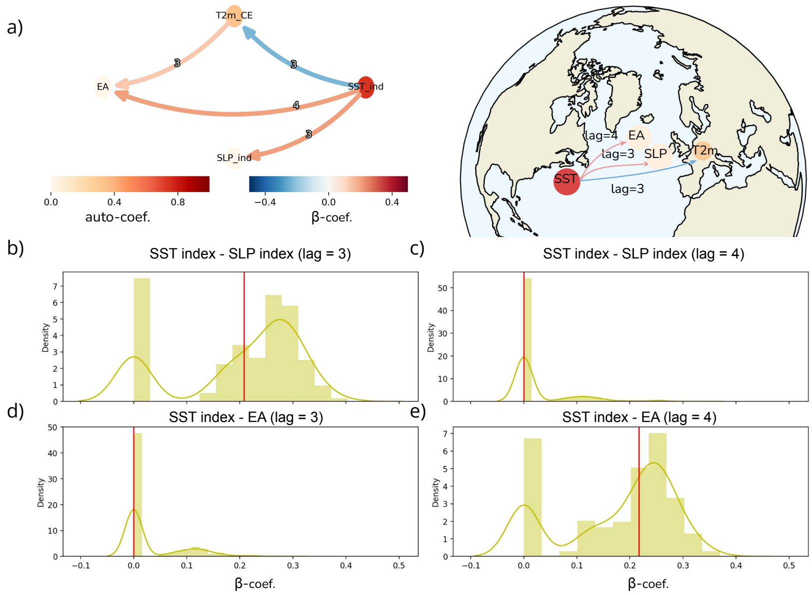

Figure 3. Causal effect network analysis for the late period (1958-2008) in ERA-20C. a) causal graph between SST index, EA teleconnection, SLP index and T2m$_{CE}$ (*left*), and schematic with illustration of the causal pathways in the Euro-Atlantic region. The strength and direction of the causal links is given by the β-coefficient and is represented by the arrows, whereas the auto-correlation path coefficient is represented for each variable by the respective circle colour. The numbers over each arrow represent the time tag (in months) when the strongest causal link between each variable pair is detected. b-e) Sensitivity of the causal links shown as the PDF of β-coefficients calculated for a random sample selection of 45 years, iterated 500 times, between the variables: SST and SLP indices at lag 3 (b) and lag 4 (c), and SST index and EA at lag 3 (d) and lag 4 (e). Only causal links with p-value < 0.1 are shown. Red lines show the correspondent β-coefficients represented in (a).

and 4 months lag). While no causal links are found in the historical simulations, we find opposite causal links than those in ERA-20C for the pi-Control simulation, suggesting an atmospheric forcing into the ocean (e.g. $\beta_{EA\rightarrow SST} \approx 0.22$), but no detected causal influence from the ocean on the atmosphere (Fig.6c).

Analysing the initialised simulations, we first exploit the full 30-member ensemble MR-30 to build a CEN for the full period (1908-2008), where each constructed timeseries thus comprises 3030 years. We find that MR-30 is able to reproduce a weakly positive SST - EA link (i.e. $\beta_{SST\rightarrow EA|SLP}$ = 0.03) at 3-month lag (Fig.6a), but not at 4-month lag as detected in ERA-20C during the late period, and in much weaker strength (i.e. $\beta_{SST\rightarrow EA|SLP}$ = 0.22, ERA-20C). No causal links from SST to EA or SLP indices are found when analysing only the late period (1958-2008). Next, we therefore investigate the causal link sensitivity to the sample size and focus on 45-year long timeseries covering the late period, allowing a direct comparison with the sensitivity analysis performed in ERA-20C (Fig.6b-e).

https://doi.org/10.5194/egusphere-2023-1412
Preprint. Discussion started: 4 August 2023

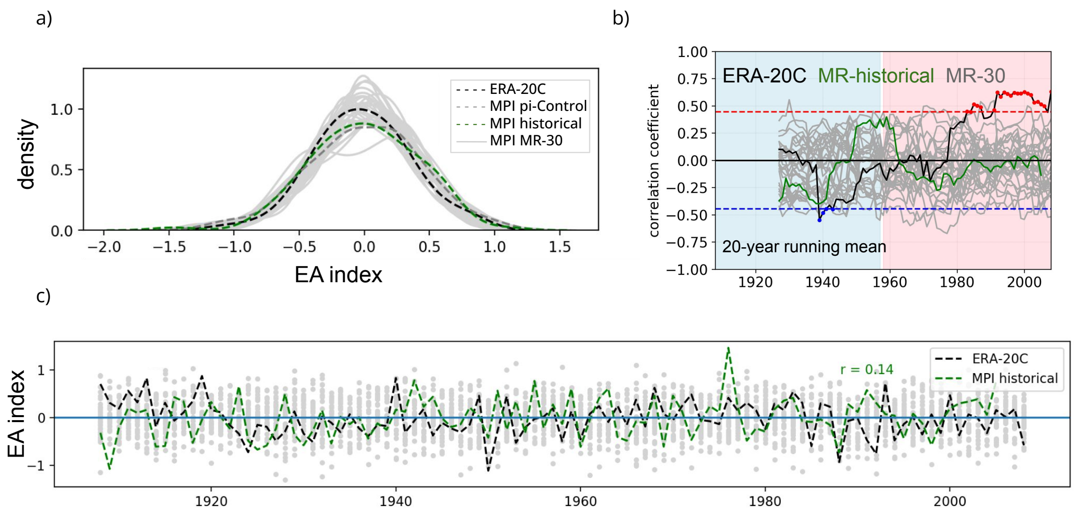

Figure 4. Model skill in reproducing summer EA and its link with spring SST. a) probability density functions (PDF) of the summer EA and c) time series of the summer EA: light grey colours in a) and c) represent individual ensemble members, and dashed grey line shows the pi-Control. b) Running-correlation between SST and EA indices for a 20-year window, for ERA-20C (black line), the ensemble mean (grey line) and the historical simulation (green line). Coloured markers indicate significant correlations at the 95% confidence interval, illustrated by the horizontal dashed lines.

3.4 Sensitivity analysis and impact on predictive skill

We perform a two-step sampling method in our sensitivity analysis with MR-30. First, 45-years are randomly selected in the late period (1958-2008). Second, one ensemble member amongst the full 30-member ensemble is randomly selected in every year. We iterate this process 2000 times, thus generating 2000 45-year-long timeseries for each SST, EA and SLP variables. In each iteration, we build one CEN to analyse whether any causal associations are detected for the sampled SST, SLP and EA timeseries. Our sensitivity results suggest that the model does mostly not reproduce the observed links between SST and EA or SLP indices (Fig.6b), showing only in very rare cases β-coefficients in the positive range as in ERA-20C (Fig.3).

We hypothesise that this MR-30 limitation in reproducing the causal links detected in ERA-20C might constrain the skillful prediction of European summers a season ahead. As a first test, we focus on two particular values of the β-coefficients, namely β_1 = -0.28 and β_2 = 0.36, corresponding to the link SST $\rightarrow$ SLP at 3-month lag illustrated by orange arrows in Fig.6b. In other words, we analyse two cases with strong causal link strength but in opposite signs, with β_2 lying in the observed ERA-20C range.

https://doi.org/10.5194/egusphere-2023-1412
Preprint. Discussion started: 4 August 2023

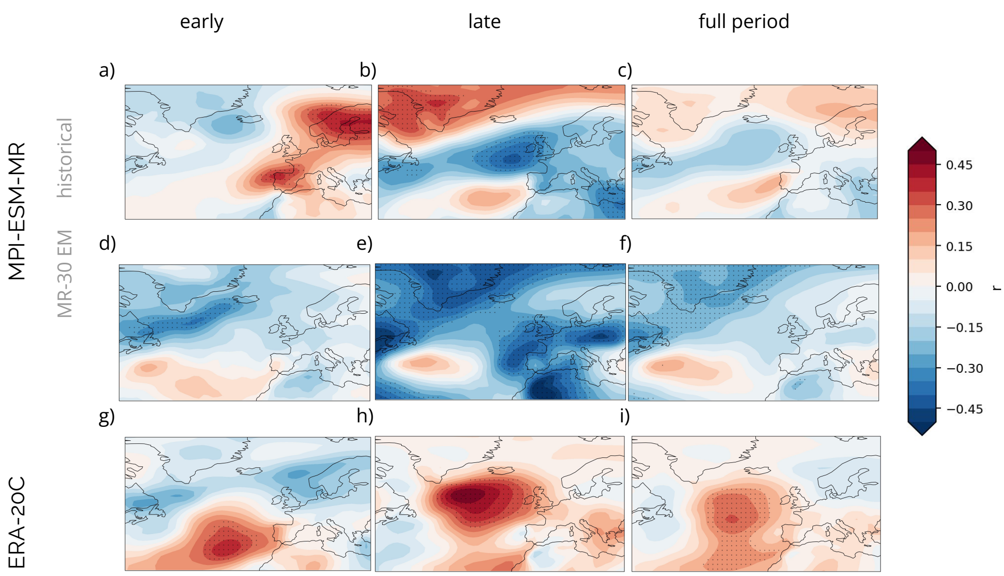

Figure 5. Comparison of the spatial characteristics of the SST-SLP relationship over the 20th century (model against ERA-20C). Correlation maps show point-wise correlation coefficients for the April-May SST index and July-August SLP means considering *early* (1908-1957; a,d,g), *late* (1958-2008; b,e,h) and *full* periods (1908-2008; c,f,i), respectively. Top row shows results for the MPI-ESM-MR historical simulation, middle row for MPI-ESM-MR 30-member ensemble, and bottom row for ERA-20C.

We perform a predictive skill assessment for each MR-30 causal timeseries respective to β_1 and β_2 against ERA-20C, checking whether the strength of the causal link has a fingerprint in the predictive skill of JA SLP. We find a better agreement between model and reanalysis for β_2 than for β_1, with significant anomaly correlation coefficients (ACC) particularly over the region where spring SST is significantly correlated to summer SLP in ERA-20C (e.g. Fig2b). However, since positive causal links are only rarely present in MR-30, we are unable to identify a robust fingerprint in the predictive skill related to any of the links between SST and EA or SLP indices.

Nevertheless, identifying a robust fingerprint of spring SST on summer predictive skill could be an important step towards targeting forecasts of opportunity (Mariotti et al., 2020). The correlation analysis in Fig.2 suggests that spring SST could influence summer T2m variability over the Euro-Atlantic region in ERA-20C during the late period (Fig.7a). Therefore, we perform an additional causality analysis in ERA-20C to highlight where in the T2m field a causal influence of spring SST is expected, and whether this causal relationship could be used to investigate an effect on MR-30's predictive skill.

We compute a causal map (Di Capua et al., 2020b) that represents the β-coefficients calculated for the link between AM SST index and each grid point of JA T2m and SLP fields, i.e. $\beta_{SST \to T2m}$ and $\beta_{SST \to SLP}$ (Fig.7b, shading and contours, respectively). We find two causal regions of opposite signs. The first region shows negative causal links and is located in northwestern Europe, partly encompassing the area used to calculate the T2m$_{CE}$ index expressed in the causal graph in Fig.3a.

https://doi.org/10.5194/egusphere-2023-1412
Preprint. Discussion started: 4 August 2023

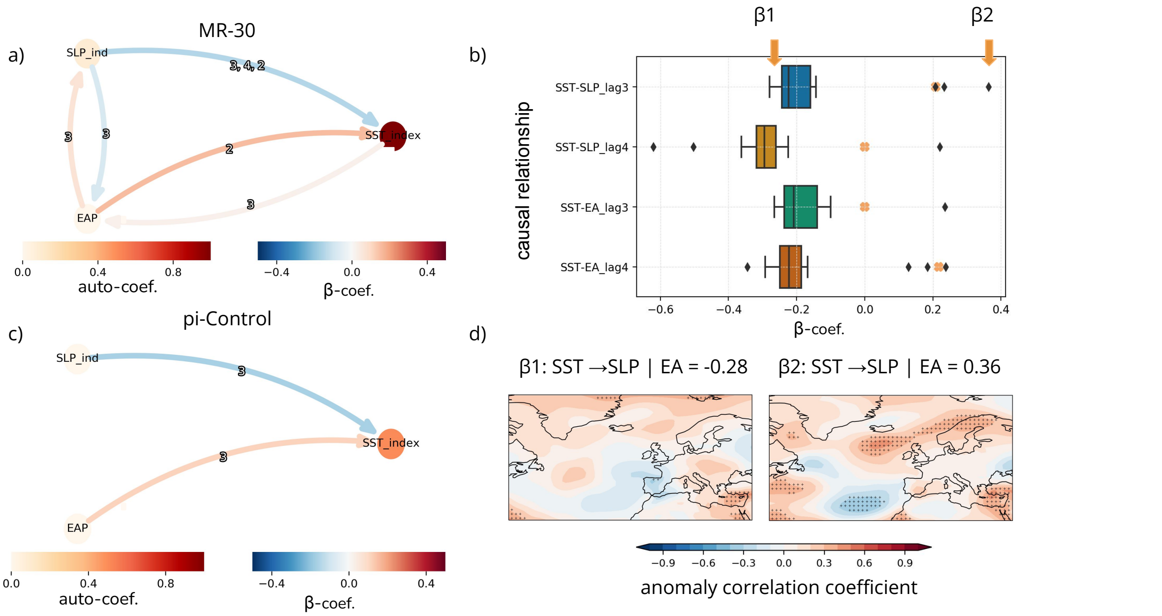

Figure 6. Causal effect networks for MPI-ESM. a) Causal graph between SST index, EA teleconnection and SLP index for the MPI-ESM-MR 30-member ensemble (MR-30) considering the full period. b) Sensitivity of the causal links between SST, SLP and EA indices at 3 and 4-month lags in the late period. Boxplots show β-coefficients calculated for a random selection of 45 years, sampling one random ensemble member amongst the 30-member set per year. This process is repeated 2000 times and only β-coefficients different from zero are shown (here denoted *MR-30 causal ensemble*). Orange "x" markers represent the β-coefficient calculated from ERA-20C (red lines in Fig.3). c) Same as (a) for a 1000-year long pi-Control simulation with MPI-ESM-MR. Only causal links with p-value < 0.1 are shown. d) Comparison of the impact on SLP predictive skill for 3-4 month lead time in MR-30 against ERA-20C for timeseries showing opposite β-coefficient strengths: a MR-30 causal timeseries with (left) β_1 = -0.28, and (right) β_2 = 0.36. Predictive skill is quantified with anomaly correlation coefficients for the late period. β_1 and β_2 are highlighted in (b) by orange arrows.

This can be interpreted as an increase of 1 SD in the spring SST index (e.g. warming over subpolar, and cooling over subtropical North Atlantic) causally driving a decrease of about 0.3 SD in the summer T2m field in northwestern Europe. The second region shows a positive causal influence on both T2m and SLP fields, reaching strong values above 0.5 for the T2m field. A black box illustrates this causal region (40°N-55°N; 15°W-34°W), denoted *Ridge*, and used to calculate the index $T2m_{Ridge}$.

Targeting this causal region, we test the hypothesis that predictive skill of the summer surface climate in MR-30 might be higher for timeseries able to reproduce the causal link strength in ERA-20C ($\beta_{SST \rightarrow T2m_{Ridge}}$ > 0.5), than for those unable to reproduce the link ($\beta_{SST \rightarrow T2m_{Ridge}}$ = 0). To test this hypothesis, we perform a two-step sampling method to generate 500 timeseries consisting of 45-years randomly selected in the ensemble space during the late period – similarly to the analysis performed for SST, EA and SLP. At 3-month lag, we find that MR-30 is able to reproduce a range of β-coefficients for SST $\rightarrow T2m_{Ridge}$, encompassing the observed link 16% of the times (Fig.7c). That is, 16% of random combinations in the MR-30

https://doi.org/10.5194/egusphere-2023-1412
Preprint. Discussion started: 4 August 2023

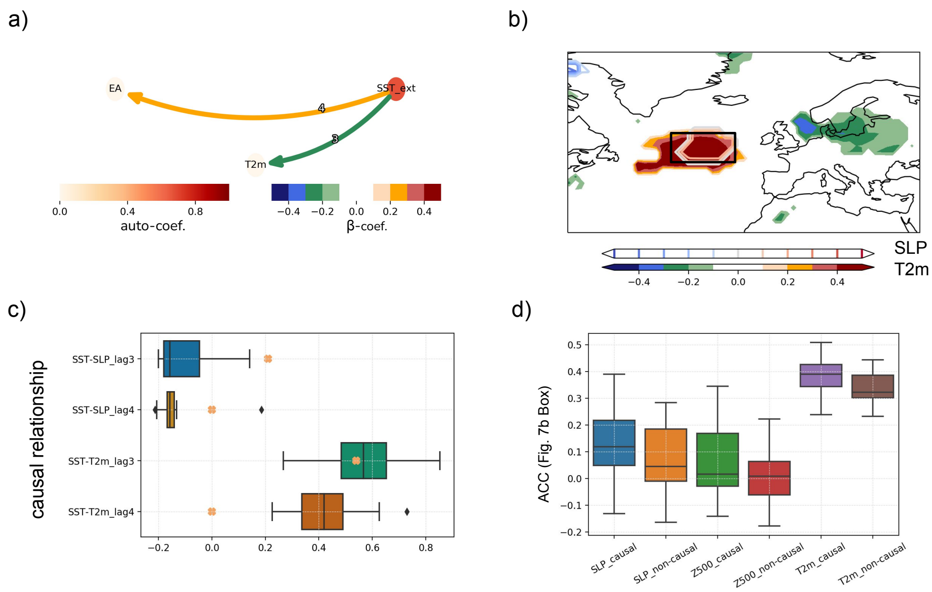

Figure 7. Spring extratropical SST causal associations and impact on MR-30 predictive skill. a) observed causal links between SST index, EA teleconnection and T2m$_{CE}$ in the late period (1958-2008); b) respective causal map for 3-month lag, showing causal links between April-May SST index and July-August temperature in shading $\beta_{SST\rightarrow T}$ and April-May SST index and July-August SLP $\beta_{SST\rightarrow SLP}$ in contours. Black box highlights the region of strongest causal influence and represents the area used to calculate the T2m index denoted $T2m_{Ridge}$ in the text. c) Sensitivity of CEN built with the SST, SLP and T2m indices for MR-30. Boxplots show β-coefficients calculated for a random selection of 45 years, sampling one random ensemble member amongst the 30-member set per year. This process is repeated 500 times and only β-coefficients different from zero are shown. Orange "x" markers represent the β-coefficient calculated for a CEN built with the SST, SLP and T2m indices from ERA-20C for the late period. Only causal links with p-value < 0.1 are shown. d) Comparison of the impact on summer surface climate predictive skill in MR-30 against ERA-20C for causal and non-causal MR-30 timeseries. Mean ACCs are shown for July-August sea level pressure (SLP), 2-metre air temperature (T2m) and 500 hPa geopotential height (Z500), averaged over the region highlighted by the grey box. See the text for further description.

https://doi.org/10.5194/egusphere-2023-1412
Preprint. Discussion started: 4 August 2023

ensemble space result in a MR-30 causal timeseries which represents a causal influence of the SST index in spring (April-May) onto the $T2m_{Ridge}$ in summer (JA).

Next, we evaluate whether the strength of this causal link is imprinted on MR-30's skill in predicting summer SLP, T2m and Z500 for the *Ridge* region a season ahead. We quantify the predictive skill with ACC using ERA-20C as a reference, for two opposite cases in MR-30: i) timeseries showing strong β-coefficients lying in the range 0.6 < β < 0.8 and ii) timeseries showing β-coefficients = 0, i.e. non-causal. We find 25 samples in i), and we therefore randomly select 25 samples in ii) to enable a direct comparison. We calculate the ACC for each of the total 50 samples, averaging over the Ridge region (Fig.7d) We find that a random selection in the ensemble space tends to show higher median and maximum values for the predictive skill of SLP, T2m and Z500 when MR-30 reproduces the causal link $SST \rightarrow T2m_{Ridge}$, than when the causal link is absent.

In summary, our predictive skill assessments conditioned to the causal influence of spring SST on both SLP (Fig.6b,d) and $T2m_{Ridge}$ (Fig.7c,d) suggest that MR-30's low performance in reproducing these causal links, in particular between spring SST and the summer EA, constrains the seasonal prediction skill of European summer climate.

4 Discussion

The framework of *forecasts of opportunity* (Mariotti et al., 2020) in seasonal prediction has been increasingly explored to identify physical processes which lead to enhanced predictability and forecast skill. Such a strategy has been particularly useful for summer (Carvalho-Oliveira et al., 2022) and winter (Dobrynin et al., 2018) seasonal predictions in the European region, where predictive skill is limited. Here, we target the summer EA to understand how its seasonal predictability is influenced by spring North Atlantic SSTs using the causal inference-based tool CEN.

Using ERA-20C, our CEN analysis confirms that the spring SST index proposed in Ossó et al. (2018) causally influences the variability of summer SLP in the Euro-Atlantic region with a 3-4 months delay during the late period. Specifically, we find that a 1 SD change in the spring SST index first drives a 0.2 SD change in the summer SLP index at 3-month lag (e.g. March-April SST → June-July SLP index), and then drives a 0.2 SD change a month later in the summer EA (e.g. March-April SST → July-August EA, Fig.3a). While EA and SLP indices are highly correlated (r = 0.82), the position of the area used to calculate the SLP index (Fig.2c) only partly overlaps the EA centre of action (Fig.1a), which extends further northwest. We speculate that the northward migration of the North Atlantic jet stream during summer (e.g. Hallam et al. (2022)) could explain the delay of a month between the causal link of SST index and EA/SLP indices.

Besides extratropical SSTs, ENSO-related tropical forcing has been suggested to influence the summer EA over more recent decades (1979 - 2016, e.g. Wulff et al. (2017); O'Reilly et al. (2018)). As opposed to the mechanism proposed in Ossó et al. (2018), Wulff et al. (2017) suggested that the summer EA is forced by diabatic heating anomalies in the tropical Pacific and Caribbean, and it is characterised by an extratropical Rossby wave train with a centre of action west of the British Isles. The CEN analysis proposed in this paper could therefore be extended to include tropical SST predictors, thus testing how the causal links discussed here could be affected by the influence of additional drivers.

Our findings suggest that the causal links detected in ERA-20C are nonstationary during the 20th century, being present only in the late period (1958-2008). Nonstationarity in teleconnections has been reported by several studies (e.g. Woollings et al. (2015); Weisheimer et al. (2019)). In particular, Rieke et al. (2021) used a 700-year pre-industrial control run with MPI-ESM-LR to investigate the tropical link of the summer EA (Wulff et al., 2017) with a statistical model, and showed that the link had a nonstationary behaviour, being present in some multidecadal epochs but not in others. Detecting nonstationarity in the causal links discussed here has an important consequence for the application on predictive skill in seasonal forecasting, implying a limited use of such causal links to target forecasts of opportunity.

Yet, our causality analysis with CEN offers an alternative assessment of MPI-ESM-MR's performance, enabling a direct comparison of the causal links reproduced by the model with those detected in reanalysis. We find that the causal links between spring SST index and summer EA and T2m are absent in pi-Control and historical simulations, but appear in some 45-year-long timeseries sampled in the initialised ensemble MR-30, thus suggesting a role of initialisation (Fig.6). We use a random ensemble subsampling to perform a predictive skill assessment conditioned to MR-30's performance in reproducing causal links between spring SST and both summer EA and $T2m_{Ridge}$. As a result, one ensemble member is randomly chosen among the 30-member per year. Alternatively, performing an ensemble subsampling to calculate an ensemble mean over a subset of ensemble members could provide a better analysis of MR-30's potential. Nevertheless, our results suggest that MR-30's limited performance in reproducing these causal links, in particular between spring SST and the summer EA, might explain its low skill in predicting summer seasonal European climate (e.g. Neddermann et al. (2018); Carvalho-Oliveira et al. (2022)).

5 Conclusions

We apply the causal inference-based tool CEN to evaluate the influence of spring North Atlantic extratropical SSTs on the predictability of summer EA and its associated impact on surface climate at seasonal timescales. Our main findings are:

- Analysing ERA-20C, we find that the observed relationship between spring SST index and summer EA is nonstationary during the 20th century, showing distinct spatial patterns between early (1902-1957) and late (1958-2008) periods. The estimated causal influence of spring SST on summer EA is of $\beta \approx 0.2$, meaning a 0.2 SD increase in EA when SST increases by 1 SD.

- We find that this relationship is only causal over the late period. A sensitivity analysis of its strength during the late period shows high variability, suggesting that the presence or absence of specific years plays an important role in the quantification of the causal link. This implies that an external physical mechanism not included in our analysis might modulate the spring SST - summer EA causal link.

- In addition to summer EA, we find that the spring SST index causally influences summer T2m ($\beta \approx$ -0.2) over a region in northwestern Europe, and the Ridge region located west of the British Isles ($\beta \approx 0.5$). This causal influence is possibly mediated by the EA.

https://doi.org/10.5194/egusphere-2023-1412
Preprint. Discussion started: 4 August 2023

– We find that pre-industrial and historical simulations of the MPI-ESM-MR do not reproduce the causal links detected in ERA-20C. In contrast, our CEN analysis with the full initialised ensemble MR-30 reveals a weakly positive causal link between spring SST and summer EA ($\beta \approx$ 0.03).

– However, for 45-year-long timeseries randomly sampled in MR-30, we find that the initialised ensemble is mostly unable to reproduce the spring SST - summer EA link.

– In contrast, MR-30 shows a moderate performance in reproducing the spring SST - summer $T2m_{Ridge}$ causal link. We find that MR-30 tends to show improved predictive skill for summer surface climate predictions over the Ridge region when the spring SST - summer $T2m_{Ridge}$ causal link is correctly reproduced by the model.

In this analysis, we demonstrate that MPI-ESM-MR has limited performance in reproducing a causal link between spring SST and summer EA amongst uninitialised and initialised model datasets. Our causality analysis therefore sheds light on the limitations of this model in providing skillful seasonal predictions of summer climate, particularly over areas which undergo a significant EA influence. Finally, our results for the initialised ensemble MR-30 show that ensemble members able to reproduce a causal link to spring SST have a potential for regional skill improvement. Our findings thereby illustrate how a causality framework could be used to target forecasts of opportunity, and highlight the importance of improving the representation of teleconnections in climate models.

Acknowledgements. The authors would like to thank Efi Rousi and Eduardo Zorita for insightful discussions at the start phase of this research. The authors also thank the Climate Modelling group at Universität Hamburg and the Climate Extremes group at VU Amsterdam for helpful discussions. Model simulations were performed using the high-performance computer at the German Climate Computing Center (DKRZ). This research was funded by the Deutsche Forschungsgemeinschaft (DFG, German Research Foundation) under Germany's Excellence Strategy—EXC 2037 'CLICCS—Climate, Climatic Change, and Society'—Project Number: 390683824, contribution to the Center for Earth System Research and Sustainability (CEN) of Universität Hamburg (J.B and L.F.B), and by the German Federal Ministry for Education and Research of Germany (BMBF) via the JPI Climate/JPI Oceans project ROADMAP (grant no. 01LP2002B) (G.D.C. and R.V.D.). J.B. was supported by Copernicus Climate Change Service, funded by the EU, under contracts C3S-330, C3S2-370.

https://doi.org/10.5194/egusphere-2023-1412
Preprint. Discussion started: 4 August 2023

References

Athanasiadis, P. J., Yeager, S., Kwon, Y.-O., Bellucci, A., Smith, D. W., and Tibaldi, S.: Decadal predictability of North Atlantic blocking and the NAO, NPJ Climate and Atmospheric Science, 3, 1–10, 2020.

Bastos, A., Janssens, I. A., Gouveia, C. M., Trigo, R. M., Ciais, P., Chevallier, F., Penuelas, J., Rödenbeck, C., Piao, S., Friedlingstein, P., et al.: European land CO 2 sink influenced by NAO and East-Atlantic Pattern coupling, Nature communications, 7, 1–9, 2016.

Carvalho-Oliveira, J., Borchert, L. F., Zorita, E., and Baehr, J.: Self-organizing maps identify windows of opportunity for seasonal European summer predictions, Frontiers in Climate, 4, 2022.

Cassou, C., Terray, L., Hurrell, J. W., and Deser, C.: North Atlantic winter climate regimes: Spatial asymmetry, stationarity with time, and oceanic forcing, Journal of Climate, 17, 1055–1068, 2004.

Cassou, C., Terray, L., and Phillips, A. S.: Tropical Atlantic influence on European heat waves, Journal of climate, 18, 2805–2811, 2005.

Comas-Bru, L. and Hernández, A.: Reconciling North Atlantic climate modes: revised monthly indices for the East Atlantic and the Scandinavian patterns beyond the 20th century, Earth System Science Data, 10, 2329–2344, 2018.

Comas-Bru, L. and McDermott, F.: Impacts of the EA and SCA patterns on the European twentieth century NAO–winter climate relationship, Quarterly Journal of the Royal Meteorological Society, 140, 354–363, 2014.

Di Capua, G., Kretschmer, M., Donner, R. V., van den Hurk, B., Vellore, R., Krishnan, R., and Coumou, D.: Tropical and mid-latitude teleconnections interacting with the Indian summer monsoon rainfall: a theory-guided causal effect network approach, Earth System Dynamics, 11, 17–34, 2020a.

Di Capua, G., Runge, J., Donner, R. V., van den Hurk, B., Turner, A. G., Vellore, R., Krishnan, R., and Coumou, D.: Dominant patterns of interaction between the tropics and mid-latitudes in boreal summer: causal relationships and the role of timescales, Weather and Climate Dynamics, 1, 519–539, 2020b.

Dobrynin, M., Domeisen, D. I., Müller, W. A., Bell, L., Brune, S., Bunzel, F., Düsterhus, A., Fröhlich, K., Pohlmann, H., and Baehr, J.: Improved teleconnection-based dynamical seasonal predictions of boreal winter, Geophysical Research Letters, 45, 3605–3614, 2018.

Domeisen, D. I., Badin, G., and Koszalka, I. M.: How predictable are the Arctic and North Atlantic Oscillations? Exploring the variability and predictability of the Northern Hemisphere, Journal of Climate, 31, 997–1014, 2018.

Duchez, A., Frajka-Williams, E., Josey, S. A., Evans, D. G., Grist, J. P., Marsh, R., McCarthy, G. D., Sinha, B., Berry, D. I., and Hirschi, J. J.: Drivers of exceptionally cold North Atlantic Ocean temperatures and their link to the 2015 European heat wave, Environmental Research Letters, 11, 074 004, 2016.

Gastineau, G. and Frankignoul, C.: Influence of the North Atlantic SST variability on the atmospheric circulation during the twentieth century, Journal of Climate, 28, 1396–1416, 2015.

Giorgetta, M., Jungclaus, J., Reick, C., Legutke, S., Brovkin, V., Crueger, T., Esch, M., Fieg, K., Glushak, K., Gayler, V., et al.: CMIP5 simulations of the Max Planck Institute for Meteorology (MPI-M) based on the MPI-ESM-LR model: The piControl experiment, served by ESGF, 2011.

Giorgetta, M. A., Jungclaus, J., Reick, C. H., Legutke, S., Bader, J., Böttinger, M., Brovkin, V., Crueger, T., Esch, M., Fieg, K., et al.: Climate and carbon cycle changes from 1850 to 2100 in MPI-ESM simulations for the Coupled Model Intercomparison Project phase 5, Journal of Advances in Modeling Earth Systems, 5, 572–597, 2013.

Hallam, S., Josey, S. A., McCarthy, G. D., and Hirschi, J. J.-M.: A regional (land–ocean) comparison of the seasonal to decadal variability of the Northern Hemisphere jet stream 1871–2011, Climate Dynamics, pp. 1–22, 2022.

https://doi.org/10.5194/egusphere-2023-1412
Preprint. Discussion started: 4 August 2023

Jungclaus, J., Fischer, N., Haak, H., Lohmann, K., Marotzke, J., Matei, D., Mikolajewicz, U., Notz, D., and Von Storch, J.: Characteristics of the ocean simulations in the Max Planck Institute Ocean Model (MPIOM) the ocean component of the MPI-Earth system model, Journal of Advances in Modeling Earth Systems, 5, 422–446, 2013.

Klavans, J. M., Cane, M. A., Clement, A. C., and Murphy, L. N.: NAO predictability from external forcing in the late 20th century, NPJ climate and atmospheric science, 4, 1–8, 2021.

Kretschmer, M., Coumou, D., Donges, J. F., and Runge, J.: Using causal effect networks to analyze different Arctic drivers of midlatitude winter circulation, Journal of climate, 29, 4069–4081, 2016.

Mariotti, A., Baggett, C., Barnes, E. A., Becker, E., Butler, A., Collins, D. C., Dirmeyer, P. A., Ferranti, L., Johnson, N. C., Jones, J., et al.: Windows of opportunity for skillful forecasts subseasonal to seasonal and beyond, Bulletin of the American Meteorological Society, 101, E608–E625, 2020.

Mauritsen, T., Stevens, B., Roeckner, E., Crueger, T., Esch, M., Giorgetta, M., Haak, H., Jungclaus, J., Klocke, D., Matei, D., et al.: Tuning the climate of a global model, Journal of advances in modeling Earth systems, 4, 2012.

Mishra, N., Prodhomme, C., and Guemas, V.: Multi-model skill assessment of seasonal temperature and precipitation forecasts over Europe, Climate Dynamics, 52, 4207–4225, 2019.

Moore, G., Renfrew, I., and Pickart, R. S.: Multidecadal mobility of the North Atlantic oscillation, Journal of Climate, 26, 2453–2466, 2013.

Neddermann, N.-C., Müller, W. A., Dobrynin, M., Düsterhus, A., and Baehr, J.: Seasonal predictability of European summer climate re-assessed, Climate Dynamics, pp. 1–18, 2018.

Oliveira, J. C., Zorita, E., Koul, V., Ludwig, T., and Baehr, J.: Forecast opportunities for European summer climate ensemble predictions using Self-Organising Maps, in: Proceedings of the 10th International Conference on Climate Informatics, pp. 67–71, 2020.

O'Reilly, C. H., Weisheimer, A., Woollings, T., Gray, L. J., and MacLeod, D.: The importance of stratospheric initial conditions for winter North Atlantic Oscillation predictability and implications for the signal-to-noise paradox, Quarterly Journal of the Royal Meteorological Society, 145, 131–146, 2019.

Ossó, A., Sutton, R., Shaffrey, L., and Dong, B.: Observational evidence of European summer weather patterns predictable from spring, Proceedings of the National Academy of Sciences, 115, 59–63, 2018.

Ossó, A., Sutton, R., Shaffrey, L., and Dong, B.: Development, Amplification, and Decay of Atlantic/European Summer Weather Patterns Linked to Spring North Atlantic Sea Surface Temperatures, Journal of Climate, 33, 5939–5951, 2020.

O'Reilly, C. H., Woollings, T., Zanna, L., and Weisheimer, A.: The impact of tropical precipitation on summertime Euro-Atlantic circulation via a circumglobal wave train, Journal of Climate, 31, 6481–6504, 2018.

Poli, P., Hersbach, H., Dee, D. P., Berrisford, P., Simmons, A. J., Vitart, F., Laloyaux, P., Tan, D. G., Peubey, C., Thépaut, J.-N., et al.: ERA-20C: An atmospheric reanalysis of the twentieth century, Journal of Climate, 29, 4083–4097, 2016.

Rieke, O., Greatbatch, R. J., and Gollan, G.: Nonstationarity of the link between the Tropics and the summer East Atlantic pattern, Atmospheric Science Letters, p. e1026, 2021.

Rousi, E., Selten, F., Rahmstorf, S., and Coumou, D.: Changes in North Atlantic atmospheric circulation in a warmer climate favor winter flooding and summer drought over Europe, Journal of Climate, 34, 2277–2295, 2021.

Rousi, E., Kornhuber, K., Beobide-Arsuaga, G., Luo, F., and Coumou, D.: Accelerated western European heatwave trends linked to more-persistent double jets over Eurasia, Nature communications, 13, 1–11, 2022.

Runge, J.: Causal network reconstruction from time series: From theoretical assumptions to practical estimation, Chaos: An Interdisciplinary Journal of Nonlinear Science, 28, 075 310, 2018.

https://doi.org/10.5194/egusphere-2023-1412
Preprint. Discussion started: 4 August 2023

Runge, J., Petoukhov, V., Donges, J. F., Hlinka, J., Jajcay, N., Vejmelka, M., Hartman, D., Marwan, N., Paluš, M., and Kurths, J.: Identifying causal gateways and mediators in complex spatio-temporal systems, Nature communications, 6, 1–10, 2015.

Runge, J., Nowack, P., Kretschmer, M., Flaxman, S., and Sejdinovic, D.: Detecting and quantifying causal associations in large nonlinear time series datasets, Science Advances, 5, eaau4996, 2019.

Schuhen, N., Schaller, N., Bloomfield, H. C., Brayshaw, D. J., Lledó, L., Cionni, I., and Sillmann, J.: Predictive Skill of Teleconnection Patterns in Twentieth Century Seasonal Hindcasts and Their Relationship to Extreme Winter Temperatures in Europe, Geophysical Research Letters, p. e2020GL092360, 2022.

Stevens, B., Giorgetta, M., Esch, M., Mauritsen, T., Crueger, T., Rast, S., Salzmann, M., Schmidt, H., Bader, J., Block, K., et al.: Atmospheric component of the MPI-M Earth system model: ECHAM6, Journal of Advances in Modeling Earth Systems, 5, 146–172, 2013.

Wallace, J. M. and Gutzler, D. S.: Teleconnections in the geopotential height field during the Northern Hemisphere winter, Monthly weather review, 109, 784–812, 1981.

Weisheimer, A., Decremer, D., MacLeod, D., O'Reilly, C., Stockdale, T. N., Johnson, S., and Palmer, T. N.: How confident are predictability estimates of the winter North Atlantic Oscillation?, Quarterly Journal of the Royal Meteorological Society, 145, 140–159, 2019.

Woollings, T., Hannachi, A., and Hoskins, B.: Variability of the North Atlantic eddy-driven jet stream, Quarterly Journal of the Royal Meteorological Society, 136, 856–868, 2010.

Woollings, T., Franzke, C., Hodson, D., Dong, B., Barnes, E. A., Raible, C., and Pinto, J.: Contrasting interannual and multidecadal NAO variability, Climate Dynamics, 45, 539–556, 2015.

Wulff, C. O., Greatbatch, R. J., Domeisen, D. I., Gollan, G., and Hansen, F.: Tropical forcing of the summer East Atlantic pattern, Geophysical Research Letters, 44, 11–166, 2017.